Effects of Preparation Method on Microstructure and Properties of UV-Curable Nanocomposite Coatings Containing Silica

Fusheng Li,[1] Shuxue Zhou,[1] Limin Wu[1,2]

[1]*Department of Materials Science and the Advanced Coatings Research Center of the China Educational Ministry, Fudan University, 220 Handan Road, Shanghai 200433, People's Republic of China*
[2]*College of Chemistry and Materials Science, Hubei University, Wuhan 430062, People's Republic of China*

Received 1 March 2005; accepted 22 March 2005
DOI 10.1002/app.21945
Published online in Wiley InterScience (www.interscience.wiley.com).

ABSTRACT: UV-curable nanocomposites were prepared by the blending method or the *in situ* method with nanosilica obtained from a sol–gel process. The microstructure and properties of the nanocomposite coatings were investigated using ^{29}Si-NMR cross-polarization/magic-angle spinning, transmission electron microscopy (TEM), Fourier transform IR (FTIR), differential scanning calorimetry (DSC), and UV–visible (UV–vis) spectra, respectively. The NMR and TEM showed that during the blending method, tetraethyl orthosilicate (TEOS) completely hydrolyzed to form nanosilica particles, which were evenly dispersed in the polymer matrix. However, for the *in situ* method, TEOS partially hydrolyzed to form some kind of microstructure and morphology of inorganic phases intertwisted with organic molecules. FTIR analysis indicated that the nanocomposites prepared from the *in situ* method had much higher curing rates than those from the blending method. DSC and UV–vis measurements showed that the blending method caused higher glass-transition temperatures and UV absorbance than the *in situ* method. © 2005 Wiley Periodicals, Inc. J Appl Polym Sci 98: 1119–1124, 2005

Key words: photopolymerization; nanocomposites; nanosilica; UV-curable coatings

INTRODUCTION

Nanocomposites are a new kind of composite materials with an ultrafine phase dispersed in 1–100 nm size,[1–5] and they show considerable improvement or novel performance compared with traditional composites. As a subdivision of nanocomposites, UV-curable nanocomposites combine the advantages of the UV-curing process and nanotechnology and therefore impart some unique properties to the materials,[6,7] finally finding potential uses in fields such as coatings, printing, inks, and adhesives.[8–10]

There are many reports on UV-curable nanocomposites,[11–18] but most of them are focused on the synthesis and characterization of nanocomposites that contain clay.[11–14] As for the UV-curable nanocomposites with nanosilica, Bauer et al.[6,16,17] successfully prepared UV-curable nanocomposites coatings with high scratch and abrasion resistance using trimethoxysilyl-terminated propyl methacrylate modified nanosilicas as the fillers. Muh et al.[7] synthesized a UV-curable hybrid nanocomposite through a sol–gel process of alkoxysilane-containing bismethacrylate-based monomers. Similarly, Soppera and Croutxe-Barghorn[9] used methacryloxypropyltrimethoxysilane as the precursor to prepare nanocomposites and studied the photopolymerization kinetics by real-time Fourier transform IR spectroscopy (FTIR).

However, up to now, the research was mainly focused on how to prepare UV-curable nanocomposites via the sol–gel process of alkoxysilane-containing monomers or the effect of nanosilica on the properties of nanocomposites. Almost no reports involved the influence of the preparation method on the microstructure and properties of UV-curable nanocomposites with nanosilica. In this study, UV-curable nanocomposites with nanosilica were prepared via the blending method or the *in situ* method. The structure of the silica phase and the photopolymeriztion kinetics of the nancomposites were investigated using ^{29}Si-NMR cross-polarization/magic-angle spinning spectroscopy (^{29}Si-NMR CP/MAS) and FTIR, respectively. The morphology and glass-transition temperature (T_g) were determined by transmission electron microscopy (TEM) and differential scanning calorimetry (DSC), respectively. The UV–visible (UV–vis) properties of the nanocomposites were measured with a UV–vis

Correspondence to: L. Wu (lxw@fudan.ac.cn).
Contract grant sponsors: Shanghai Special Nano Foundation, Doctoral Foundation of University, Trans-Century Outstanding Talented Person Foundation of the China Educational Ministry, and Key Project of the China Educational Ministry.

TABLE I
Recipes for Preparation of Nanocomposite Coatings

Sample code	Recipe (g)							
	TEOS	$NH_3 \cdot H_2O$[a]	H_2O	EtOH	EA	MPS	TMPTA	Irgacure 651
BU	17.3	1.13	2.9	34.5	45	0	50	3
BM	17.3	1.13	2.9	34.5	45	5	45	3
IU	17.3	1.13	2.9	34.5	45	0	50	3
IM	17.3	1.13	2.9	34.5	45	5	45	3
Pure polymer	0	0	0	0	45	0	55	3

[a] Ammonia solution with 25–28% ammonia content.

spectrophotometer. The objective of this study was to explore the possible influence of preparation methods on the microstructure and properties of nanocomposites.

EXPERIMENTAL

Materials

Tetraethyl orthosilicate (TEOS) and 3-(trimethoxysilyl) propyl methacrylate (MPS) were purchased from Shanghai Huarun Chemical Company of China and Degussa, respectively. *N*-Butyl acetate (≥99.0%), absolute ethanol (EtOH), and ammonia solution (25–28% ammonia content) were purchased from Shanghai Chemical Reagent Corporation. 2,2-Dimethoxy-1,2-diphenylethan-1-one (Irgacure 651) was a gift of Ciba Specialty Chemicals. Trimethylolpropane triacrylate (TMPTA) and epoxy acrylate (EA, weight-average molecular weight = 1000, viscosity = 30,000 mPa s at 60°C) were the products of Changxing Corporation (Kunshan, China) and Sanmu Corporation (Yixing, China), respectively. All materials were used as received without further purification.

Preparation of EA/SiO_2 nanocomposite coatings

The UV-curable nanocomposite coatings were prepared by two methods: the blending method and the *in situ* method.

Blending method

Colloidal silica particles with an average size of 40 nm were prepared by the sol–gel method according to Suratwala et al.,[19] using a molar ratio of 9 : 0.2 : 2.5 : 1 for EtOH/NH_3/H_2O/TEOS. TEOS and fractional absolute alcohol were charged into a three-necked round-bottomed flask and then dropped into a mixture of residual absolute alcohol, deionized water, and ammonia within 0.5 h and stirred at 50°C for 8 h. The prepared colloidal silica was modified with MPS based on a 3 : 14 weight ratio of MPS/TEOS at 50°C for 6 h. The modified or unmodified silica was then mixed with EA and TMPTA by vigorous stirring for 0.5 h, followed by heating to 80°C to evaporate water and ethanol within 80 min.

In situ method

A mixture of EA, TEOS, and fractional absolute alcohol were charged into a three-necked round-bottomed flask and dropped into a mixture of residual absolute alcohol, deionized water, and ammonia at 50°C over 0.5 h and continuously stirred for 8 h. Then, MPS was added based on a 3:14 weight ratio of MPS/TEOS and stirred for another 6 h. The molar ratio of EtOH/NH_3/H_2O/TEOS was the same as that used in the blending method. The modified or unmodified silica was directly mixed with TMPTA by vigorous stirring for 0.5 h and then heated to 80°C to evaporate water and ethanol within 80 min. Table I summarizes the recipes for the preparation of nanocomposite coatings and the sample codes. The symbols B and I represent the blending and *in situ* methods, respectively, and U and M indicate unmodified silica and modified silica with MPS, respectively.

After adding Irgacure 651, the obtained UV-curable nanocomposite coatings were cast on glass or quartz substrates with a drawdown rod. Then, they were irradiated with a UV-curing apparatus (UV Crosslinker, Spectroline Company) with a wavelength of 365 nm and an intensity of 2.8 mW/cm^2. The thickness of obtained nanocomposite coating was approximately 20 μm.

Characterization

^{29}Si-NMR CP/MAS spectra

The ^{29}Si-NMR CP/MAS spectra were recorded on a Bruker MSL300 at a pulse duration of 4.5 s, a contact time of 1.5 ms, and a pulse spacing of 6 s. The sample was placed in a rotator made of ZrO_2. Centrifugation at a magic angle was performed at a spinning frequency of 8.4 kHz.

TEM observation

TEM micrographs were taken with a Hitachi H-600 apparatus (Hitachi Corp., Tokyo). Samples were pre-

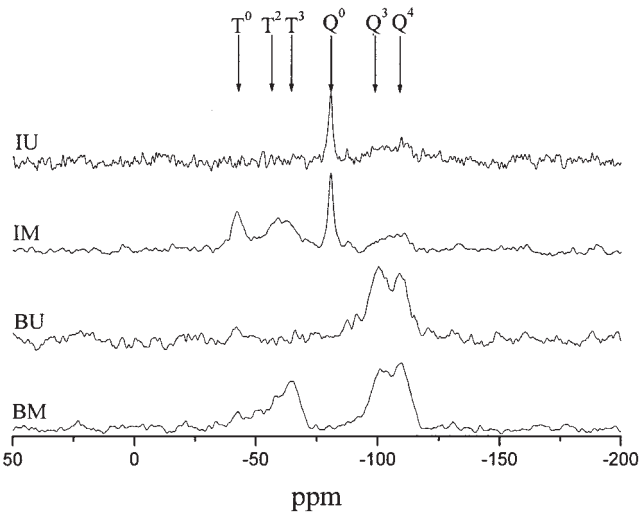

Figure 1 ^{29}Si-NMR CP/MAS spectra of IU, IM, BU, and BM samples, where B and I represent the blending and *in situ* methods, respectively, and U and M indicate unmodified silica and modified silica with MPS, respectively.

pared by ultramicrotome at room temperature, giving nearly 100-nm thick sections. No further staining was used to improve the contrast. The image analyses were performed with Photoshop 7.0 software.

FTIR spectra

The FTIR spectra of samples before curing and after different UV-curing times were scanned by a Magna-IR 550 spectrometer (Nicolet Instruments, Madison, WI). In this study, sandwichlike NaCl plates were used for the FTIR scanning to minimize the influence of oxygen in the atmosphere.

DSC analysis

DSC thermograms were recorded using a modulated DSC 2910 (TA Instruments, New Castle, DE) under a nitrogen atmosphere in a temperature range of 25–150°C at a heating rate of 10°C/min.

UV–vis spectra

The absorbance and transmittance spectra of the nanocomposite coatings with 200–700 nm wavelengths were recorded by a UV–vis spectrophotometer (Hitachi UV-3000).

RESULTS AND DISCUSSION

Structure of silica phase in nanocomposites

Figure 1 shows the ^{29}Si-NMR spectra of UV-cured nanocomposite coatings. Samples BM and BU have obvious Q^3 and Q^4 structures but no Q^0 structure, indicating a high hydrolysis of TEOS during the blending method. In addition, the BM sample shows a T^3 structure, indicating that MPS has been successfully grafted to the surface of nanosilica particles. However, for the IU and IM samples, the Q^3 and Q^4 structures are not seen whereas the Q^0 structure can be clearly observed, suggesting that TEOS only partially hydrolyzes during the *in situ* method. This is possibly attributable to the relatively slow hydrolyzing rate, which results from the high viscosity of the reaction system in the presence of oligomer EA and/or the poor compatibility between the oligomer and TEOS. In addition, for the IM sample, besides T^2 and T^3 structures, a T^0 structure can be clearly noted, indicating only part of the MPS hydrolyzed and condensed with the silica phase in the *in situ* method.

Morphology of nanocomposites

Figure 2 demonstrates the morphology of the nanocomposite coatings prepared by the blending method and the *in situ* method. The nanosilica particles can be clearly seen for the blending method [Fig. 2(a,b)]. However, for the *in situ* method, there are no distinct nanosilica particles observed and the phases observed by TEM seem to be some loose inorganic structures or a partial inorganic phase intertwisted with some organic segments [Fig. 2(c,d)]. This is probably because the nanosilica particles have already been formed for the blending method; but for the *in situ* method the existence of oligomers (EA) remarkably impairs the hydrolysis of TEOS, resulting in no individual silica particles. Note also from Figure 2 that the BM [Fig. 2(b)] and IM [Fig. 2(d)] samples have better silica phase dispersion than the BU [Fig. 2(a)] and IU [Fig. 2(c)] samples, showing that the introduction of MPS can greatly improve the dispersion of the silica phase in the UV-curable EA coatings for both the blending and *in situ* methods.

Photopolymerization kinetics of nanocomposites

The typical FTIR spectra of UV-curable nanocomposite coatings with different irradiation times are illustrated in Figure 3. The intensity of the peak at 1635 cm^{-1} for the C═C stretching vibration decreases with increasing exposure time under UV irradiation. Because the peak at 1635 cm^{-1} is well separated from the other peaks, it is usually used to quantify the conversion of C═C bonds in UV-curable coatings, with the peak at 1725 cm^{-1} being due to C═O stretching absorbance as the reference for its invariability during UV curing.[20] Thus, the conversion of C═C bonds can be calculated according to the following equation:

$$C\ (\%) = 100 \times (1 - A_t S_0 / A_0 S_t) \qquad (1)$$

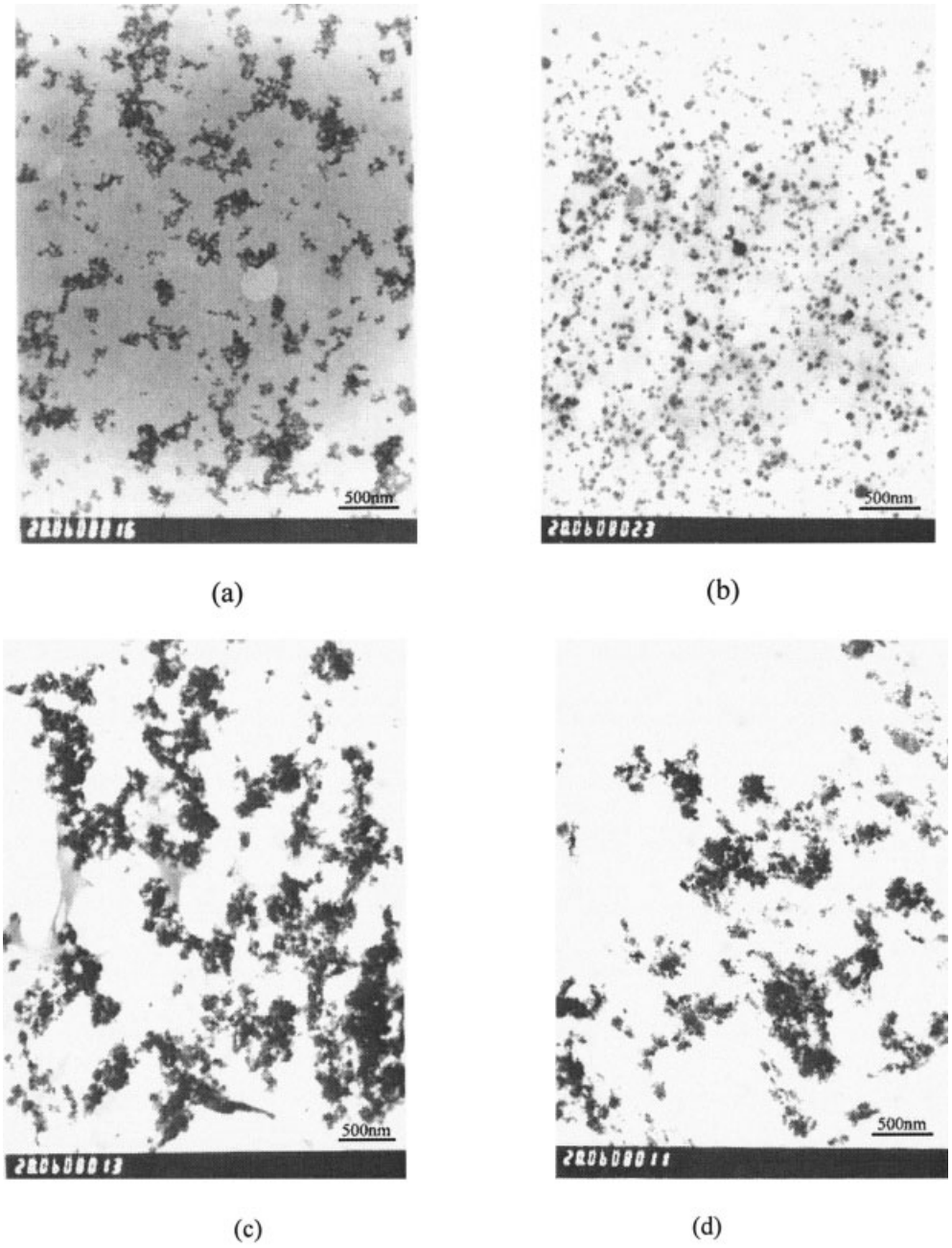

Figure 2 TEM pictures of the (a) BU, (b) BM, (c) IU, and (d) IM samples, where B and I represent the blending and *in situ* methods, respectively, and U and M indicate unmodified silica and modified silica with MPS, respectively.

where A_t and A_0 are the areas of the peak at 1635 cm^{-1} and S_t and S_0 are the areas of the peak at 1725 cm^{-1} at irradiation time t ($t = 0$).

Based on the data calculated by eq. (1), Figure 4 plots the conversion curves for the UV-curable nanocomposite coatings containing nanosilica and prepared by different methods. After a negligible induction time at the beginning of the photopolymerization, an accelerated polymerization is observed because of the gel effect; then, the polymerization slows down because of the vitrification of the resin. This is the typical kinetic curve of UV-curable polymers with three functionality reactive dilutes,[20] suggesting that the introduction of nanosilica obviously does not change the photopolymerization kinetics of pristine EA.

Figure 4 also indicates that the IU and IM samples have faster curing rates than the BU and BM samples. This is probably attributable to the following two factors: there is more water to be adsorbed and trapped in the silica phase because of the strong affinity of inorganic SiO_2 to water during the blending method due to more hydrolysis of TEOS than during the *in situ* method, so the water remaining in the UV-curable

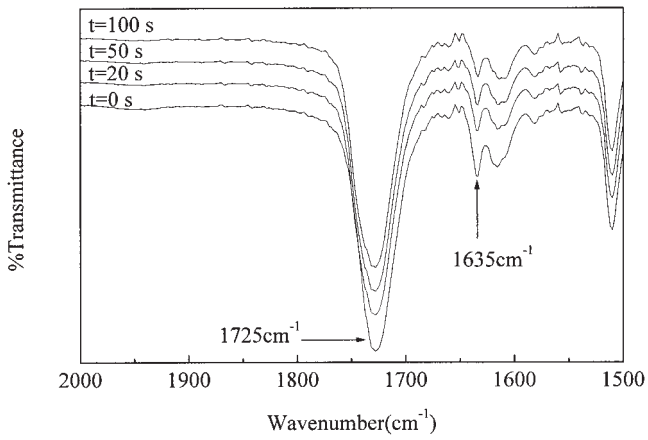

Figure 3 The FTIR spectra for the BM sample cured with different irradiation times, where B represents the blending method and M indicates modified silica with MPS.

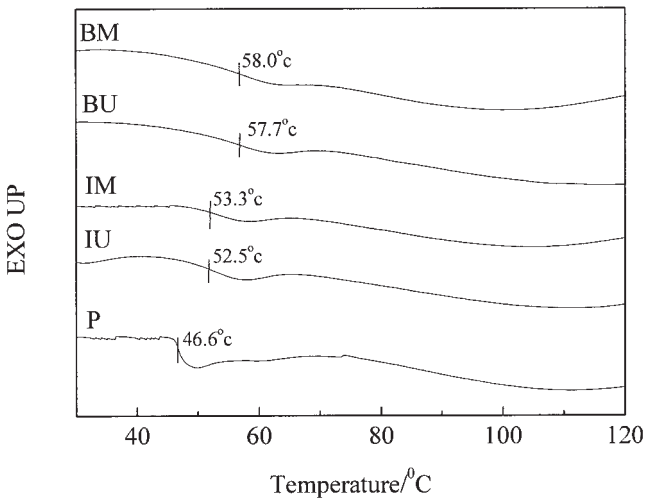

Figure 5 The DSC curves for pristine EA and the nanocomposites.

nanocomposite coatings inhibits photopolymerization[21]; and the microstructure and morphology of some inorganic phases intertwisted with organic molecules during the *in situ* method, as shown in Figure 2(c,d), which decreases the probability of bimolecular termination of polymer radicals, resulting in an increasing photopolymerization rate.[9] Samples BM and IM have faster curing rates than corresponding samples BU and IU, respectively, probably because the C═C bond of MPS is more reactive than that from TMPTA because MPS is easier to move than TMPTA.

Glass-transition temperature of nanocomposites

Figure 5 demonstrates the DSC curves of the nanocomposites. All nanocomposites have higher T_g values than pristine EA because incorporating nanosilica particles can decrease the mobility of polymer chains. Samples BU and BM have much higher T_g values than the corresponding IU and IM, suggesting that the blending method is favorable for increasing the interaction between the inorganic and organic phases of the UV-curable nanocomposites because of the higher surface area of nanosilica particles that are formed. MPS modification seems to have no obvious impact on the T_g values of the nanocomposites.

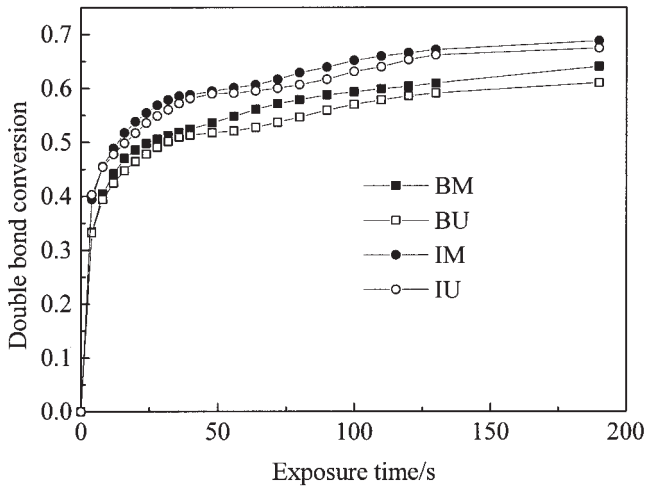

Figure 4 The photopolymerization kinetic curves of tnanocomposite coatings.

Optical properties of nanocomposites

The optical properties of nanocomposites are critical to their application in some fields such as optical fiber coatings, lens coatings, and so forth.[7] The weather resistance of nanocomposite coatings also depends on their optical properties,[22] especially their absorbance in the UV range. Figure 6 illustrates the UV–vis spectra of the nanocomposite coatings.

In the range of 400–700 nm wavelengths (visible light), more than 90% transmittance for pristine EA and all nanocomposite coatings is observed, indicating that introduction of nanosilica does not reduce the transmittance of UV-cured coatings. However, in the range of 290–400 nm (UV rays), the transmittance of the nanocomposites decreases dramatically. The UV absorbance decreases in the order of BM > BU > IM > IU > pure polymer, suggesting nanosilica can shield UV rays, and evenly dispersed nanosilica particles from the blending method seem to enhance the UV shielding property more efficiently than the loose silica structure from the *in situ* method.

CONCLUSIONS

UV-curable nanocomposites were prepared using the blending method and the *in situ* method. During the

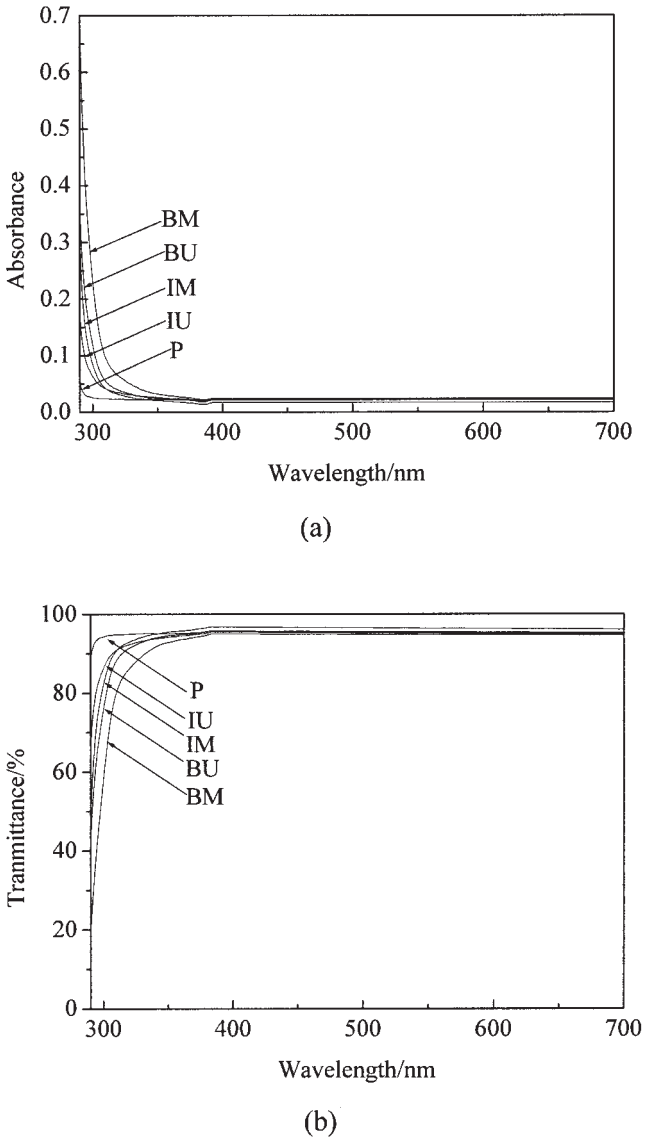

Figure 6 The UV–vis spectra of the nanocomposite coatings: (a) absorbance and (b) transmittance.

blending method, TEOS completely hydrolyzed to form nanosilica particles, which were evenly dispersed in the polymer matrix. However, for the *in situ* method, TEOS only partially hydrolyzed to form inorganic phases intertwisted with organic molecules.

The nanocomposites prepared by the *in situ* method had much higher curing rates than those from the blending method, but the latter had greater glass-transition temperatures and UV shielding property than the former because the blending method caused uniformly dispersed nanosilica particles whereas the *in situ* method did not.

The authors thank Shanghai Special Nano Foundation, the Doctoral Foundation of University, the Trans-Century Outstanding Talented Person Foundation of the China Educational Ministry, and the Key Project of the China Educational Ministry for the financial support of this research.

References

1. Benfarhi, S.; Decker, C.; Keller, L.; Zahouily, K. Eur Polym J 2004, 40, 493.
2. Bauer, F.; Glasel, H. J.; Decker, U.; Ernst, H.; Freyer, A.; Hartmann, E.; Sauerland, V.; Mehnert, R. Prog Org Coat 2003, 47, 147.
3. Becker, O.; Varley, R. J.; Simon, G. P. Eur Polym J 2004, 40, 187.
4. Torre, L.; Frulloni, E.; Kenny, J. M.; Manferti, C.; Camino, G. J Appl Polym Sci 2003, 90, 2532.
5. Dong, W.; Zhu, C. Mater Lett 2000, 45, 336.
6. Bauer, F.; Ernst, H.; Decker, U.; Findeisen, M.; Glasel, H. J.; Langguth, H.; Hartmann, E.; Mehnert, R.; Peuker, C. Macromol Chem Phys 2000, 201, 2654.
7. Muh, E.; Stieger, M.; Klee, J. E.; Frey, H.; Mulhaupt, R. J Polym Sci Part A: Polym Chem 2001, 39, 4274.
8. Wenning, A. Macromol Symp 2002, 187, 597.
9. Soppera, O.; Croutxe-Barghorn, C. J Polym Sci Part A: Polym Chem 2003, 41, 716.
10. Decker, C. Polym Int 1998, 45, 133.
11. Vollath, D.; Szabo, D. V. Adv Eng Mater 2004, 3, 117.
12. Uhl, F. M.; Davuluri, S. P.; Wong, S. C.; Webster, D. C. Chem Mater 2004, 16, 1135.
13. Decker, C.; Zahouily, K.; Keller, L.; Benfarhi, S.; Bendaikha, T.; Baron, J. J Mater Sci 2002, 37, 4831.
14. Benfarhi, S.; Decker, C.; Keller, L.; Zahouily, K. Eur Polym J 2004, 40, 493.
15. Glasel, F. H. J.; Bauer, F.; Ernst, H.; Findeisen, M.; Hartmann, E.; Langguth, H.; Mehnert, R.; Schubert, R. Macromol Chem Phys 2000, 201, 2765.
16. Bauer, F.; Sauerland, V.; Glasel, H. J.; Ernst, H.; Findeisen, M.; Hartmann, E.; Langguth, H.; Marquardt, B.; Mehnert, R. Macromol Mater Eng 2002, 287, 546.
17. Bauer, F.; Sauerland, V.; Ernst, H.; Glasel, H. J.; Naumov, S.; Mehnert, R. Macromol Chem Phys 2003, 204, 375.
18. Andrzejewska, E. Prog Polym Sci 2001, 26, 605.
19. Suratwala, T. I.; Hanna, M. L.; Miller, E. L.; Whitman, P. K.; Thomas, I. M.; Ehrmann, P. R.; Maxwell, R. S. J Non-Cryst Solids 2003, 316, 349.
20. Wang, J. Z. Y.; Bogner, R. H. Int J Pharm 1995, 113, 113.
21. Li, F.; Zhou, S.; You, B.; Wu, L. J Appl Polym Sci 2005, 96, 912.
22. Skaja, A. D.; Croll, S. G. Polym Degrad Stabil 2003, 79, 123.